A Deep Dive into classical and Topological CFT Thermodynamics in Lifshitz and Hyperscaling Violating Black Holes

Mohammad Ali S. Afshar,[1,2,3,*] Mohammad Reza Alipour,[2,1,†] Saeed Noori Gashti,[2,‡] and Jafar Sadeghi[1,3,§]

[1] *Department of Physics, Faculty of Basic Sciences, University of Mazandaran P. O. Box 47416-95447, Babolsar, Iran*

[2] *School of Physics, Damghan University, P. O. Box 3671641167, Damghan, Iran*

[3] *Canadian Quantum Research Center, 204-3002 32 Ave Vernon, BC V1T 2L7, Canada*

(Dated: June 13, 2025)

To effectively utilize the AdS/CFT correspondence, a precise set of rules must be established to guide the translation of computed quantities in the gravitational sector into their CFT counterparts, and vice versa. This framework is commonly referred to as the holographic dictionary. The formulation of such dictionaries opens a two-way gateway, allowing researchers to extend theoretical principles and findings from one domain into the other for further exploration and study. The development of a holographic dictionary for Lifshitz black holes and hyperscaling violation (HSV) models [1] has provided an essential foundation for studying CFT thermodynamics and phase behavior of these black holes. Based on this framework, we will investigate their thermodynamic properties using two distinct approaches. In the first step, we adopt the classical and traditional method, identifying critical points to examine the behavior of the free energy function as a function of temperature near the critical boundary. By analyzing its behavior, we will study phase transitions and then proceed to evaluate the stability of the models. In the next step, to compare both methodologies and highlight their equivalence—particularly demonstrating the accessibility of the topological method compared to the classical approach—we will analyze phase behavior through the lens of topological charges.

Keywords: AdS/CFT correspondence, Thermodynamic Topology, Stability

CONTENTS

I. Introduction 2

II. Lifshitz and hyperscaling violating black holes 3

III. Stability 8

IV. Thermodynamic Topology 10
A. $\theta = 0.5$, $C_{crt} = 2.23$ 12
B. $\theta = 0$, $C_{crt} = 6.613$ 13
C. $\theta = -0.5$, $C_{crt} = 20.678$ 14

V. Conclusion 15

VI. Appendix 15
A. $\theta = 0.5, \overline{Q}_{crt} = 0.00269$ 16
B. $\theta = 0, \overline{Q}_{crt} = 0.000907$ 17
C. $\theta = -0.5, \overline{Q}_{crt} = 0.00029$ 18

References 18

* m.a.s.afshar@gmail.com
† mr.alipour@stu.umz.ac.ir
‡ saeed.noorigashti@stu.umz.ac.ir; saeed.noorigashti70@gmail.com
§ pouriya@ipm.ir

I. INTRODUCTION

The gauge/gravity duality, or AdS/CFT correspondence, states that a gravitational theory formulated in an asymptotically Anti-de Sitter (AdS) space is equivalent to a conformal field theory (CFT) defined at its boundary. This means that every phenomenon occurring in the gravitational sector within the AdS framework—including black hole physics—can be described in an equivalent manner within the dual CFT. This correspondence serves as a powerful tool, akin to a golden key, for studying complex quantum dynamics in strongly coupled systems such that calculations that are difficult to perform directly in gravitational theory may be more manageable in the corresponding CFT, and vice versa. The existence of this duality allows researchers to strategically tackle challenging problems in high-energy physics and quantum gravity with greater flexibility. Despite its intricate nature, the core concept of this correspondence seems to stem from a fundamental logical principle: any phenomena occurring in higher-dimensional spaces must remain interpretable within lower dimensions at the boundary, subject to constraints. To aids in intuition and conceptual understanding and in a simplified analogy, one could compare this idea to classical mathematical principles such as Gauss's divergence theorem (which translates three-dimensional to two-dimensional interpretations) and Stokes' theorem (mapping two-dimensional to one-dimensional properties), both of which find applications in electromagnetic gauge fields (Gauss's and Ampère's laws).
However, beyond the theoretical foundation, the critical aspect lies in the practical realization and application of this duality. To make use of this correspondence, a precise set of rules must be established to guide the translation of quantities computed in the gravity sector to their CFT counterparts, and vice versa. These translation rules are commonly referred to as the "holographic dictionary". For example, the partition function of the gravitational theory can be equated to the generating function of the dual CFT [2]. Among the most compelling applications of the AdS/CFT framework is its usage to the study of black hole physics, which are considered ideal scenarios for coupling gravity to gauge fields, such as electromagnetism. Despite the experimental inaccessibility and the predominantly theoretical nature of black hole studies, they remain remarkable candidates for investigating this duality. In particular, black hole thermodynamics, given its minimal reliance on relativistic complexities, may serve as the optimal context. On one hand, when the CFT is at a finite temperature, it represents a thermal system—analogous to standard thermodynamics in any field theory. On the other hand, in the AdS context, black holes exhibit well-defined thermodynamic properties such as:
• Temperature, derived from Hawking radiation
• Entropy, associated with the event horizon area
• Energy (or mass), computed using general relativity and quantum field theory in curved spacetime.
Thus, leveraging our golden duality, we can effectively translate the thermodynamic behavior of an AdS black hole into the language of its dual CFT. Under this framework:
• The black hole temperature in the bulk corresponds to the CFT temperature in finite volume.
• The entropy computed from the black hole's horizon maps onto the thermal entropy in the CFT.
Also, Similar correspondences can be established for other thermodynamic variables. For instance:
• The gravitational action computed on the boundary of black hole spacetime can be linked to the free energy of the thermal dual CFT.
• In holographic CFTs dual to Einstein gravity, the central charge is related to both the AdS radius and Newton's constant, implying that changes in central charge within the CFT can lead to variations in both the cosmological constant and Newton's constant in the gravity sector. Consequently, varying the cosmological constant in the gravity side is dual to varying the central charge or the number of colors in the dual gauge theory. Therefore, the central charge and its conjugate chemical potential (also known as color susceptibility) play an essential role in the holographic dual of extended black hole thermodynamics [3–5].

However, not everything follows this direct mapping, as certain complications arise. For example, bulk pressure is not dual to the pressure of the field theory, or Black hole thermodynamic volume does not correspond to the spatial volume of the CFT formulation [6]. Fortunately, these issues can be addressed by introducing new thermodynamic variables, which help refine the CFT interpretation of extended black hole thermodynamics [7, 8].

While the derivation of these holographic dictionaries is inherently complex, they unlock new perspectives for studying lower-dimensional boundary physics. For instance, in the Gauss–Bonnet model, the formulation of a holographic dictionary enabled investigations into CFT thermodynamics across different dimensions, yielding valuable insights into dimensional constraints [9, 10]. In this regard, recent studies aimed at constructing a holographic dictionary for Lifshitz and hyperscaling violating black holes [1] motivated us to investigate the CFT thermodynamics of these black holes from two perspectives: 1. The general and traditional method, 2. A novel topological approach.

Most black hole models proposed for study are inherently theoretical due to the lack of direct experimental verification. Based on prior knowledge, experience, and available data, researchers hope that if spacetime geometry follows Riemannian principles and the prevailing mechanics remain relativistic, certain constructed models will closely align with

cosmic reality. Given these assumptions, it is natural to expect such models to exhibit familiar physical behaviors. However, what makes theoretical black hole models particularly intriguing is the potential emergence of novel gravitational-gauge behaviors, which arise from the interplay between gravitational corrections and modern gauge fields. These behaviors may not form in classical, Earth-bound conditions but can manifest under extreme astrophysical scenarios. And that's what motivates us to study these behaviors. Black hole thermodynamics is no exception to this phenomenon. For instance, it has been widely observed that AdS black holes, where the cosmological constant is treated as pressure [3], exhibit distinct small-to-large black hole phase transitions, akin to the gas-liquid transition in Van der Waals fluids [11–13]. Additionally, the generalized Euler relation is recovered in restricted phase space [14].

Accordingly,in the general and traditional method, parameters in the CFT space are first defined according to the holographic dictionary, followed by the computation of critical points and the Gibbs free Energy, enabling the analysis of phase behavior based on temperature.

Meanwhile, a recently developed approach introduces a mapping of the energy function into a two-dimensional space (r, Θ), opening a new avenue for studying black hole behavior. This technique allows for the investigation of vector field behavior in mapped space with respect to the computation of winding numbers, yielding interesting insights into geodesic structures and black hole thermodynamics [15–55].

To illustrate the behavioral similarities and provide a visual comparison of both approaches—and recognizing that in cases where one method (traditional or topological) may be difficult to apply, the other could serve as a suitable alternative—we will employ both approaches in analyzing CFT thermodynamics for Lifshitz and hyperscaling violating black holes. We also will investigate black holes across various parametric scenarios, assessing potential differences in behavior, analyzing their phase dynamics, and ultimately proposing a behavioral classification based on topological charges.

Accordingly, in this article we will begin by introducing the models, their general parameters, and constraints. We will then proceed with the traditional thermodynamic approach, analyzing phase diagrams based on swallowtail structures or smooth continuous phase transitions. Subsequently, we will explore the stability and topological method and its application in black hole thermodynamics, and finally, we will synthesize and conclude our findings.

II. LIFSHITZ AND HYPERSCALING VIOLATING BLACK HOLES

Lifshitz black holes emerged in 2008–2009 as gravitational solutions modeling anisotropic scaling between time and space, inspired by Lifshitz fixed points in condensed matter physics. In these early models, the bulk geometry was altered to display an anisotropic scaling between time and space—represented by a dynamical critical exponent "z", where time scales as $t \to \lambda^z t$ and space as $x \to \lambda x$. This idea was initially driven by the need to construct gravitational duals for certain condensed matter systems, where such anisotropic scaling is a defining feature. Kachru and his colleagues, in the foundational work, introduced these spacetimes in string theory to holographically describe non-relativistic quantum critical systems [56, 57]. Early 2010, researchers recognized that many strongly correlated systems showed even more complex scaling behavior that could not be captured by the exponent "z" alone. This led to the introduction of an additional parameter —the hyperscaling violation exponent(HSV) θ to capture broader scaling violations in thermodynamic properties, often arising in Einstein-Maxwell-Dilaton theories studied by researchers like Dong, Harrison, and Charmousis [58]. Including θ in the gravitational models modifies the overall scaling of the metric so that physical quantities in the dual field theory scale anomalously. These hyperscaling violating black holes allow one to incorporate richer thermodynamic and hydrodynamic behaviors, making them especially relevant for studying phase transitions, transport phenomena, and quantum criticality in non-relativistic systems. These two solutions extend the AdS/CFT correspondence to systems without conformal symmetry, such as strange metals or high-temperature superconductors. Lifshitz metrics model anisotropic criticality, while hyperscaling violation modifies thermodynamic scaling, crucial for describing real-world condensed matter systems. They enable studies of transport properties (e.g., conductivity), entanglement entropy, and phase transitions in holographic frameworks.

An interesting point to note is that they can also coexist ($z \neq 1, \theta \neq 0$), but the distinction lies in whether the emphasis is on anisotropic spacetime symmetry (Lifshitz) or effective dimensionality (HSV).

Lifshitz black holes features

For the spherical form of this black hole, Table I presents the parametric constraints along with their corresponding physical implications.

Case	Physical Meaning	Thermo condition	Holographic Dual	Stability
$z=1$	Relativistic AdS black holes	Specific heat can be positive (stable)	CFTs	Stable(AdS/CFT framework)
$z>1$	Spacetime becomes non-relativistic (time scales faster than space)	Specific heat can be positive (stable) if spatial dimensions d compensate	Lifshitz field theories	Stable if NEC holds
$z<1$	Time scales slower than space, leading to potential instabilities, Unphysical or exotic	Specific heat often becomes negative, leading to thermodynamic instability	Rarely viable	Unstable (ghosts, tachyons)

TABLE I. Lifshitz black holes

HSV black holes features

Furthermore, Table II presents the parametric constraints along with their corresponding physical implications with respect to the spherical form of black hole

Case	Physical Meaning	Thermo condition	Holographic Dual	Stability
$z=1$,$\theta=0$	Relativistic AdS black holes	Specific heat can be positive (stable)	CFTs	Stable(AdS/CFT framework)
$z>1$,$\theta=0$	Spacetime becomes non-relativistic (time scales faster than space)	Specific heat can be positive (stable) if spatial dimensions d compensate	Lifshitz field theories	Stable if NEC holds
$0<\theta<d$, $z\geq 1+\theta/d$	Hyperscaling violation,Mimics quantum critical systems with effective dimensional reduction	NEC condition: $(d-\theta)(z-1-d/\theta)\geq 0$	Dual to quantum critical systems violating hyperscaling.eg: spin liquids, disordered phases.	depends to condition
$\theta=d$ z Not allowed	Naked singularity or Unphysical spacetime	NEC condition:Violated	No consistent dual theory	Unphysical
$\theta<0$	Requires exotic matter (e.g., nonlinear gauge fields)	Possible only with exotic matter	Speculative duals: Hypothetical "emergent" higher-dimensional theories (e.g., glassy phases).	Often unstable.

TABLE II. HSV black holes

The general line element describing Lifshitz and hyperscaling violating black holes in $(d+1)$-dimensions can be expressed as [1],

$$ds^2=\chi(r)\left[-\left(\frac{r}{L}\right)^{2z}f(r)dt^2+L^2\frac{dr^2}{f(r)r^2}+r^2d\Omega^2_{k,d-1}\right], \tag{1}$$

where the function $\chi(r)$ is defined as $\chi(r)=\left(\frac{r}{r_F}\right)^{-\frac{2\theta}{d-1}}$. For large values of r, the function $f(r)$ asymptotically approaches unity, i.e., $f(r)\to 1$ as $r\to\infty$. This metric has been proposed as a holographic dual to states in Lifshitz invariant field theories that exhibit hyperscaling violation. In the special case where $z=1$ and $\theta=0$, the geometry reduces to asymptotically Anti-de Sitter (AdS) spacetime. The parameter k determines the topology of spatial slices at constant t and r, taking values: $k=-1$ for hyperbolic topology, $k=0$ for planar topology, $k=1$ for spherical topology. The analytic solutions describing these black holes are given by the metric above and generalize previously known solutions [1],

$$f(r)=\frac{(d-2)^2L^2}{r^2(d-\theta+z-3)^2}-\frac{m}{r^{d-\theta+z-1}}+\frac{q^2}{r^{2(d-\theta+z-2)}}+1 \tag{2}$$

In [60] researcher extend the charged spherical black hole solutions with Lifshitz asymptotics ($\theta \neq 0$) . Also, in[61] they study incorporate arbitrary Lifshitz scaling and hyperscaling violation parameters in charged black branes with non-trivial topology. with respect to [1], we have,

$$L^2 = -\frac{r_0^{\frac{2\theta}{d-1}}((d-\theta+z-2)(d-\theta+z-1))}{2\Lambda_0 r_F^{\frac{2\theta}{d-1}}} \tag{3}$$

and

$$\rho_3^2 = \frac{r_F^{\frac{2\theta}{d-1}}\left(2q^2(d-\theta-1)(d-\theta+z-3)\right)}{Z_0 L^{2z} r_0^{\gamma\lambda_3}} \tag{4}$$

Considering L as the bulk curvature radius (analogous to the AdS curvature radius) and r_0 as an arbitrary length scale, this solution holds under the conditions $d-\theta+z-3>0$ and $\theta<d-1$. The corresponding black hole parameters include: ADM mass (M), Hawking temperature (T) are as follows,

$$M = \frac{m(d-\theta-1)L^{-z-1}r_F^{\theta}\omega_{k,d-1}}{16\pi G} \tag{5}$$

$$T = \frac{r^z\left(\frac{(d-2)^2L^2}{r^2(d-\theta+z-3)} - \frac{q^2(d-\theta+z-3)}{r^{2(d-\theta+z-2)}} + d-\theta+z-1\right)}{4\pi L^{z+1}} \tag{6}$$

The horizon radius r_h is defined as the largest positive root of f(r) = 0. The mass M depends on the parameters (m, L, r_F), where m can be further expressed in terms of r_h, L, and q by solving $f(r_h, L, m, q) = 0$ for m. To establish a generalized Smarr relation and the first law, we express M as a function of the thermodynamic variables S and Q, along with the analog of the 'bulk pressure' $P := -\Lambda_0/8\pi G$ in the EMD theory [59]. Here, Λ_0 represents the 'bare' cosmological constant appearing in the Lagrangian. Due to its coupling to the dilaton, Λ_0 does not correspond to the pressure of a bulk perfect fluid in the conventional sense of the cosmological constant, yet we retain P as a useful theoretical parameter. Also, entropy and charge of these model can be considered as,

$$S = \frac{r^{d-\theta-1}r_F^{\theta}\omega_{k,d-1}}{4G} \tag{7}$$

$$Q = \frac{\rho_3 Z_0 L^{z-1}\omega_{k,d-1}r_F^{\frac{\theta-2\theta}{d-1}}}{16\pi G} \tag{8}$$

The central charge C can be inferred from the proportionality constant in the grand canonical free energy expression:$F = M - TS - \Phi Q$. Since mass, entropy, and charge scale with C (i.e., $M, S, Q \propto C$), its holographic dictionary entry can be determined by analyzing entropy expressions. The Bekenstein-Hawking entropy can be rewritten in terms of the scaling properties: $S \propto Cx^{d-\theta-1}$, where $x = r_h/L$, indicating as then the central charge C defines as,

$$C = \frac{AL^{d-\theta-1}r_F^{\theta}}{G} \tag{9}$$

Also, with respect to [1], we will have

$$\bar{Q} = QL^{2-z}r_F^{\frac{\theta}{d-1}}r_0^{-\frac{\theta}{d-1}+z-1} \tag{10}$$

The internal energy and temperature dictionary entries arise from symmetry considerations. The bulk quantities ML and TL are dimensionless, and should correspond to boundary quantities that remain invariant under,

$$\bar{E}R^{\frac{z-\theta}{\frac{(d-1)(1-\theta)}{d-1}}} = LM \tag{11}$$

and

$$\bar{T}R^{\frac{z-\theta}{\frac{(d-1)(1-\theta)}{d-1}}} = LT \tag{12}$$

So, we will have,

$$S = \overline{S} = \frac{C x^{d-\theta-1}\omega_{k,d-1}}{4A} \tag{13}$$

where A is a constant. To derive the internal energy expression for the conformal field theory (CFT), we introduce dimensionless parameters that facilitate a more systematic formulation of thermodynamic quantities,

$$x = \frac{r_h}{L} \tag{14}$$

By applying the relationships established in Eqs. (5), (7), (9), (11), we obtain a comprehensive framework for evaluating thermodynamic properties of the CFT. So we will have,

$$\begin{aligned}\bar{E} = &-\frac{R^{-\frac{z-\theta}{(d-1)(1-\theta)}}\left(C(d-\theta-1)\omega_{k,d-1}x^{d-\theta+z-1}\right)}{16\pi A}\\ &\times\left(-\frac{128\pi^2A^2\bar{Q}^2r_F^{2\theta-\frac{2\theta}{d-1}}x^{-2(d-\theta+z-2)}r_0^{\gamma\lambda_3+\frac{2\theta}{d-1}-\frac{2dz}{d-1}+\frac{2z}{d-1}+\frac{2d}{d-1}-\frac{2}{d-1}}}{C^2Z_0(d-\theta-1)(d-\theta+z-3)\omega_{k,d-1}^2}-\frac{(d-2)^2}{x^2(d-\theta+z-3)^2}-1\right)\end{aligned} \tag{15}$$

Also, temperature is calculated as,

$$\begin{aligned}\bar{T} = &\frac{x^z R^{-\frac{z-\theta}{(d-1)(1-\theta)}}}{4\pi}\\ &\times\left(-\frac{128\pi^2A^2\bar{Q}^2r_F^{2\theta-\frac{2\theta}{d-1}}x^{-2(d-\theta+z-2)}r_0^{\gamma\lambda_3+\frac{2\theta}{d-1}-\frac{2dz}{d-1}+\frac{2z}{d-1}+\frac{2d}{d-1}-\frac{2}{d-1}}}{C^2Z_0(d-\theta-1)\omega_{k,d-1}^2}+\frac{(d-2)^2}{x^2(d-\theta+z-3)}+d-\theta+z-1\right)\end{aligned} \tag{16}$$

Furthermore, the critical points of the system can be determined using the following conditions, $\frac{\partial\tilde{T}}{\partial x}\Big|_{\overline{Q},C}=0$, $\frac{\partial^2\tilde{T}}{\partial x^2}\Big|_{\overline{Q},C}=0$. Utilizing Eq. (16), we extract the precise locations of these critical points.

$$x_{crt}^2 = \frac{(d-2)^2(2-z)}{z(d-\theta+z-2)(d-\theta+z-1)} \tag{17}$$

As shown in the Eq. (17), the critical expression is independent of both the CFT framework and the central charge parameter. So, with respect to the above concepts, the $\bar{Q}^2{}_{crt}$ is calculated as follows,

$$\begin{aligned}\bar{Q}^2{}_{crt} = &C^2z^3Z_0\left(-\frac{(d-2)^2(z-2)}{z(d-\theta+z-2)(d-\theta+z-1)}\right)^{d-\theta+z}\omega_{k,d-1}^2r_F^{-\frac{2(d-2)\theta}{d-1}}r_0^{-\gamma\lambda_3-\frac{2\theta}{d-1}+2z-2}\\ &\times\frac{(d-\theta-1)(d-\theta+z-2)^2(d-\theta+z-1)^3}{128\pi^2A^2(d-2)^4(z-2)^2(d-\theta+z-3)(2d-2(\theta+2)+z)}\end{aligned} \tag{18}$$

Finally, employing the formulations in equations (7), (15) and (16), we determine the Helmholtz free energy, which serves as a key thermodynamic potential for characterizing the stability and equilibrium properties of the CFT,

$$\bar{F} = \bar{E} - S\bar{T} \tag{19}$$

Also, we can obtain,

$$\bar{F} = \frac{CR^{\frac{z-\theta}{\theta-1}}\omega_{k,d-1}x^{d-\theta+z-1}\left(\frac{128\pi^2A^2\bar{Q}^2(2d-2\theta+z-4)r_F^{\frac{2(d-2)\theta}{d-1}}x^{-2(d-\theta+z-2)}r_0^{\gamma\lambda_3+\frac{2\theta}{d-1}-2z+2}}{c^2Z_0(d-\theta-1)(d-\theta+z-3)\omega_{k,d-1}^2}-\frac{(d-2)^2(z-2)}{x^2(d-\theta+z-3)^2}-z\right)}{16\pi A} \tag{20}$$

According to Figs 1-4, we can examine the first and second order phase transitions for a black hole in the CFT thermodynamic state. In Fig. 1 and 2, we analyzed the scenario with a fixed central charge, examining the electric charge both above and below its critical values. For $\overline{Q} < \overline{Q}_{crt}$, the free energy exhibits a swallowtail behavior, indicating a first-order phase transition between two thermodynamically stable branches. The horizontal branch with lower entropy corresponds to the small black hole, and the vertical branch with higher entropy corresponds to the large black hole. In contrast, the middle

branch connecting these two branches is unstable due to its negative heat capacity. Also, for $\overline{Q} = \overline{Q}_{crt}$, we have a second-order phase transition, and the small stable black hole directly transforms into a large stable black hole. However, when $\overline{Q} > \overline{Q}_{crt}$, no phase transition takes place. In Fig. 3 and 4, we examine the charge $\overline{Q}$ fixed and different values of central charge above and below the critical points. For $C > C_{crt}$, there is a first-order phase transition, for $C = C_{crt}$ there is a second-order phase transition, and for $C < C_{crt}$ there is no phase transition.

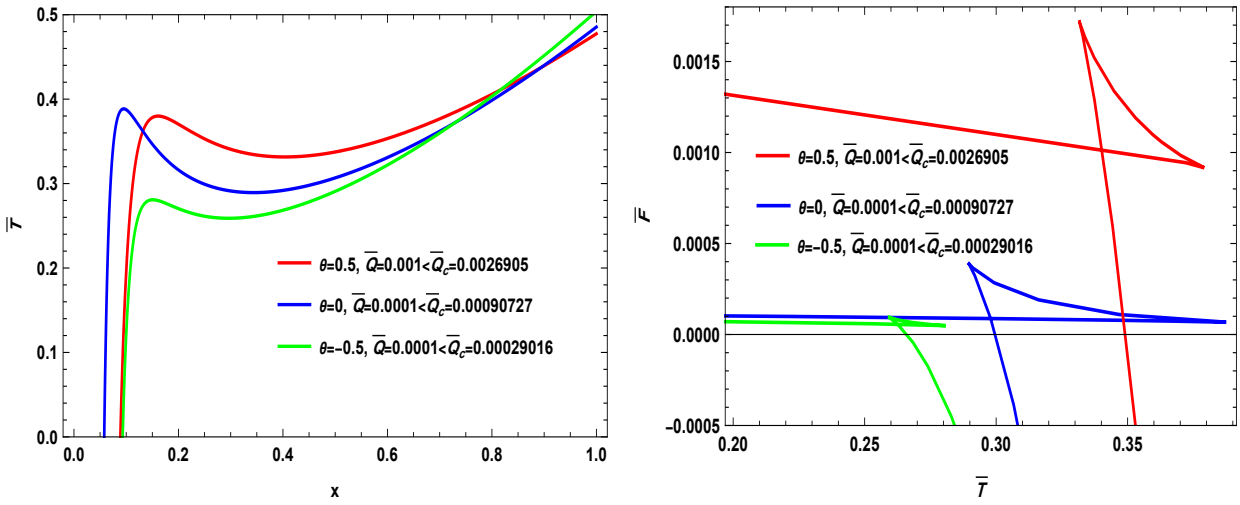

(a) (b)

FIG. 1. The each plot illustrates three distinct values of θ, while other parameters are fixed as follows: $k = Z_0 = \gamma = \lambda_3 = R = r_0 = r_F = A = \omega_{k,d-1} = 1$, $C = 2$, $z = 3/2$, and $d = 4$. (a) temperature vs. x and (b) free energy vs. temperature

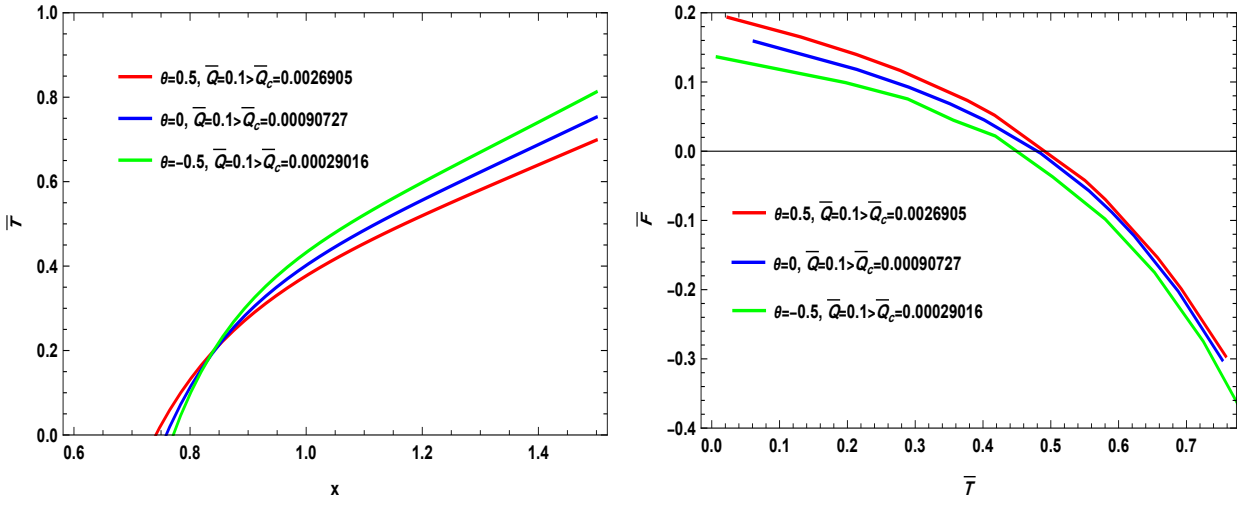

(a) (b)

FIG. 2. The each plot illustrates three distinct values of θ, while other parameters are fixed as follows: $k = Z_0 = \gamma = \lambda_3 = R = r_0 = r_F = A = \omega_{k,d-1} = 1$, $C = 2$, $z = 3/2$, and $d = 4$. (a) temperature vs. x and (b) free energy vs. temperature

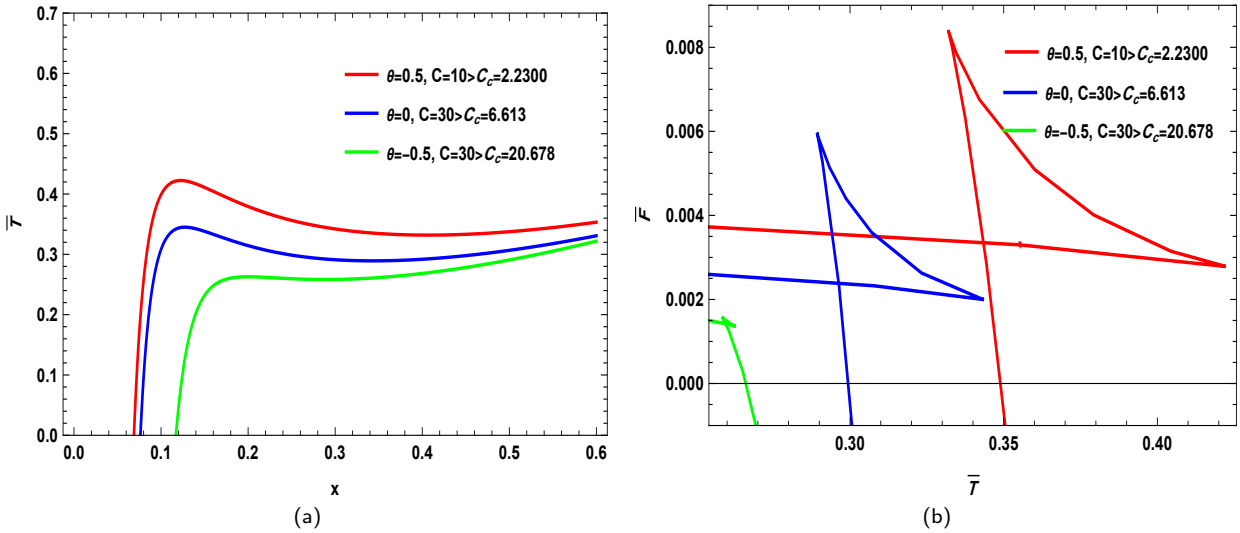

FIG. 3. The each plot illustrates three distinct values of θ, while other parameters are fixed as follows: $k = Z_0 = \gamma = \lambda_3 = R = r_0 = r_F = A = \omega_{k,d-1} = 1$, $\overline{Q} = 0.003$, $z = 3/2$, and $d = 4$. (a) temperature vs. x and (b) free energy vs. temperature

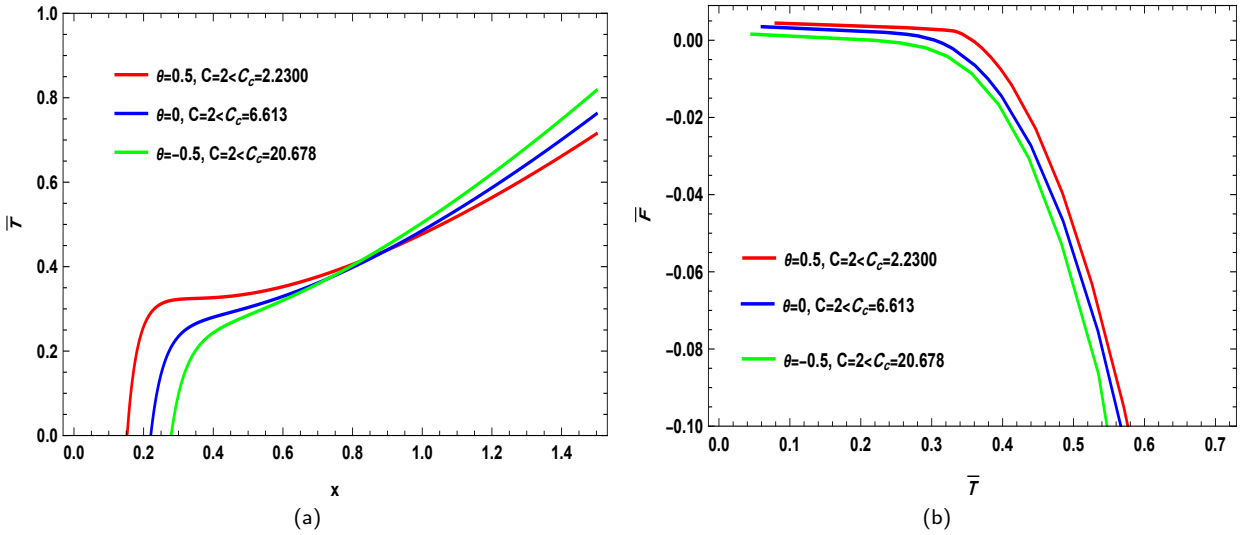

FIG. 4. The each plot illustrates three distinct values of θ, while other parameters are fixed as follows: $k = Z_0 = \gamma = \lambda_3 = R = r_0 = r_F = A = \omega_{k,d-1} = 1$, $\overline{Q} = 0.003$, $z = 3/2$, and $d = 4$. (a) temperature vs. x and (b) free energy vs. temperature

III. STABILITY

To gain deeper insights into the thermodynamic properties and stability of the dirty black hole, we examine the specific heat at constant parameters. The specific heat can be computed via the thermodynamic relation,

$$\widetilde{C} = \overline{T}\left(\frac{\partial S}{\partial \overline{T}}\right) = \overline{T}\left(\frac{\partial S}{\partial x}\right)\left(\frac{\partial x}{\partial \overline{T}}\right). \tag{21}$$

So, we can calculate the $\widetilde{C}$ using the Hawking temperature from Eq. (16) and entropy from Eq. (7),

$$\widetilde{C} = \frac{C(d-\theta-1)x^{d-\theta+1}\omega_{k,d-1}\left(-\frac{128\pi^2A^2\overline{Q}^2 r_F^{\frac{2(d-2)\theta}{d-1}} x^{-2(d-\theta+z-2)} r_0^{\gamma\lambda_3+\frac{2\theta}{d-1}-2z+2}}{C^2Z_0(d-\theta-1)\omega_{k,d-1}^2} + \frac{(d-2)^2}{x^2(d-\theta+z-3)} + d-\theta+z-1\right)}{4A\left(\frac{128\pi^2A^2\overline{Q}^2(2d-2\theta+z-4) r_F^{\frac{2(d-2)\theta}{d-1}} x^{-2(d-\theta+z-3)} r_0^{\gamma\lambda_3+\frac{2\theta}{d-1}-2z+2}}{C^2Z_0(d-\theta-1)\omega_{k,d-1}^2} + x^2z(d-\theta+z-1) + \frac{(d-2)^2(z-2)}{d-\theta+z-3}\right)} \tag{22}$$

This formulation of the specific heat reveals several key features of the black hole's thermodynamic behavior: A second-order phase transition occurs, at the points where the specific heat diverges. This signifies a fundamental change in the thermal properties of the black hole. When some region, the specific heat is positive, indicating thermal stability and some other region, the specific heat becomes negative, signifying thermal instability. These findings are consistent with our topological analysis, where configurations with positive winding numbers correspond to thermally stable states, while negative winding numbers indicate instability. The specific heat, demonstrating that black holes experience enhanced thermal stability. This dependence implies that the stability of the system strengthens significantly as the black hole size increases.

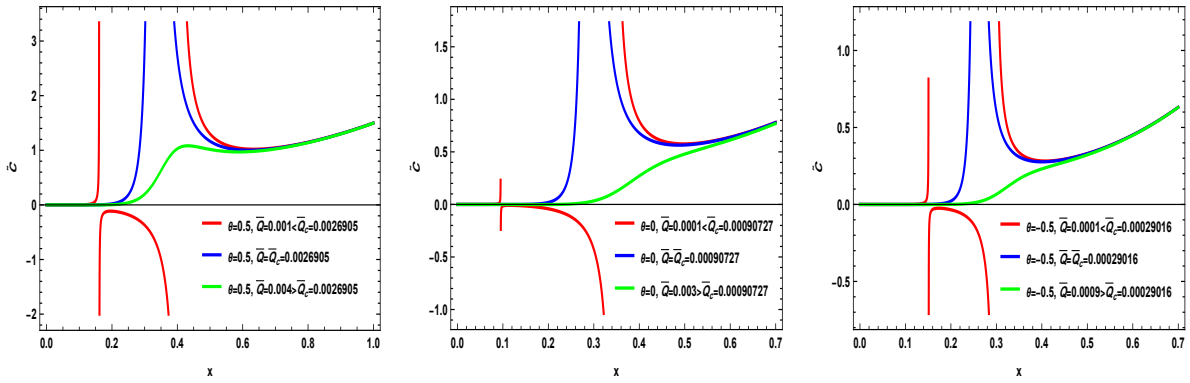

FIG. 5. The stability plot $(\widetilde{C}-x)$ (Heat capacity) for different free parameters $k = Z_0 = \gamma = \lambda_3 = R = r_0 = r_F = A = \omega_{k,d-1} = 1$, $C = 2$ $z = 3/2$, and $d = 4$.

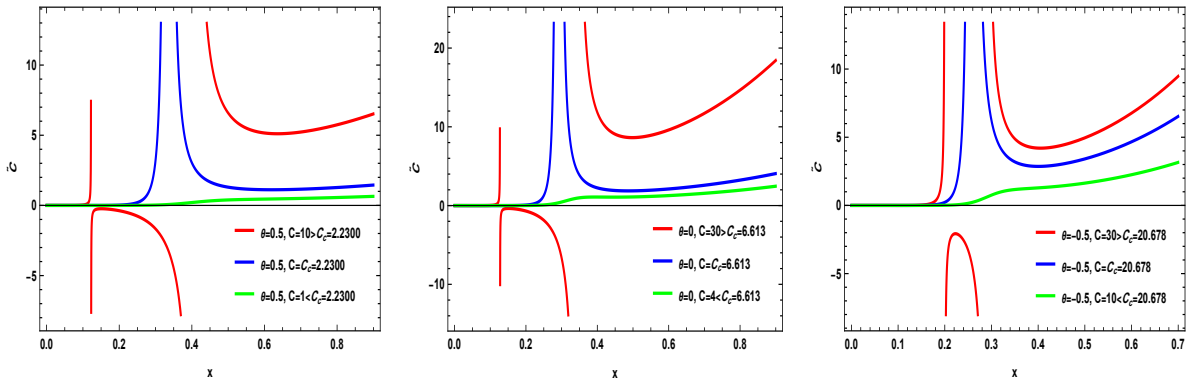

FIG. 6. The stability plot $(\widetilde{C}-x)$ (Heat capacity) for different free parameters $k = Z_0 = \gamma = \lambda_3 = R = r_0 = r_F = A = \omega_{k,d-1} = 1$, $\overline{Q} = 0.003$ $z = 3/2$, and $d = 4$.

As shown in Fig. 5, for different values of the free parameter—particularly $\overline{Q}$—the system exhibits instability or negative values only within a very small range where $\overline{Q} < \overline{Q}_c$. However, at all other points, it maintains a positive value, indicating stability. This behavior is clearly visible in Fig. 5. Conversely, the parameter C exhibits the opposite trend. Specifically,

except for a narrow range where $C > C_{crt}$ Fig. 6, the system demonstrates instability with negative values. Yet, at most points, it remains stable. This contrast in the structural behavior of $\overline{Q}$ and C is well illustrated in the study of the thermodynamic topology of black holes, particularly in the context of first-order and second-order phase transitions.

IV. THERMODYNAMIC TOPOLOGY

The integration of topology into black hole thermodynamics provides a powerful framework for analyzing phase transitions. By assigning specific topological indices to critical points in the phase space, this method uncovers novel classifications and behaviors that conventional thermodynamic analyses might overlook. The foundation of this approach lies in the generalized Helmholtz free energy, which serves as a key tool for evaluating stability and transition dynamics. The generalized Helmholtz free energy, an extension of the traditional Helmholtz free energy, incorporates off-equilibrium effects and is defined as,

$$F(S,V,Y) = U(S,V,Y) - TS. \tag{23}$$

Here, S represents entropy, V denotes volume, Y accounts for additional thermodynamic degrees of freedom, T is the temperature, and U is the internal energy. Within the framework of conformal field theory (CFT) thermodynamics, the phase behavior of black holes can be characterized using the Helmholtz free energy expression $\overline{F} = E - \overline{TS}$. This formulation encapsulates the relationship between energy, temperature, and entropy in the thermodynamic analysis of black hole systems. A deeper understanding of thermodynamic topology requires analyzing the modified Helmholtz free energy function, which is given by [15–52],

$$\mathcal{F} = M - \frac{S}{\tau}. \tag{24}$$

Here, M represents the black hole mass, while τ corresponds to the inverse temperature period in the Euclidean formulation. To investigate the phase structure of black holes using conformal field theory (CFT) thermodynamics, we reformulate the generalized Helmholtz energy within the CFT framework as [47],

$$\overline{\mathcal{F}} = E - \frac{\overline{S}}{\overline{\tau}}. \tag{25}$$

In this formulation, the Helmholtz energy attains an on-shell condition exclusively when the time parameter satisfies $\overline{\tau} = \overline{\tau}_H = \frac{1}{T_h}$. This constraint ensures consistency with holographic thermodynamics, reinforcing the connection between black hole phase transitions and the underlying conformal field dynamics. Examining the topological features of this function reveals a vector structure,

$$\boldsymbol{\phi} = (\phi^{r_h}, \phi^{\Theta}), \tag{26}$$

where ϕ^{r_h} is derived from the derivative of F with respect to r, and ϕ^{Θ} contains angular dependencies influencing phase stability. This vector can be reformulated as,

$$\boldsymbol{\phi} = ||\boldsymbol{\phi}|| e^{i\Theta}. \tag{27}$$

Applying topological field theory, the normalized vector n^a is constructed as,

$$n^a = \frac{\phi^a}{|\boldsymbol{\phi}|}, \tag{28}$$

which allows defining the antisymmetric superpotential governing thermodynamic phase transitions,

$$V^{\mu\nu} = \frac{1}{2\pi} \epsilon^{\mu\nu\rho} \epsilon^{ab} n^a \partial_\rho n^b. \tag{29}$$

Using Duan's method, the associated topological current emerges as,

$$j^\mu = \frac{1}{2\pi} \epsilon^{\mu\nu\rho} \epsilon^{ab} \partial_\nu n^a \partial_\rho n^b. \tag{30}$$

This topological current remains conserved due to Noether's theorem,

$$\partial_\mu j^\mu = 0. \tag{31}$$

By analyzing zero points of j^{μ}, one can determine the winding number,

$$W=\sum_{i=1}^{n}\beta_i\eta_i=\sum_{i=1}^{n}\omega_i. \tag{32}$$

This index captures the intricate topological features of black hole phase transitions by quantifying the mapping of thermodynamic variables in phase space. The Hopf index β_i measures vector linking behaviors, while ω_i encapsulates rotational properties of the field structure. Through these topological invariants, black hole thermodynamics acquires a more refined classification scheme, offering deeper insights into its fundamental nature.
Given these premises and considering Eqs. (15) and (25), the general form of the quantities required for the topological study of the model will be as follows,

$$\begin{aligned}\overline{\mathcal{F}}=&-\frac{R^{-\frac{z-\theta}{1-\theta}}\omega_{k,d-1}(-1-\frac{(d-2)^2}{x^2(d-\theta+z-3)^2}-\frac{128r_F^{2\theta-\frac{2\theta}{d-1}}r_0^{\frac{-2zd+2d+2\theta+2z-2}{d-1}+\lambda_3\gamma}\overline{Q}^2x^{4-2d-2z+2\theta}\pi^2A^2}{\omega_{k,d-1}^2(d-\theta+z-3)(d-\theta-1)C^2Z_0})(d-\theta-1)x^{d-\theta+z-1}C}{16A\pi}\\&-\frac{x^{d-\theta-1}C\omega_{k,d-1}}{4A\tau}\end{aligned} \tag{33}$$

We can calculate the ϕ^x and ϕ^{Θ} with respect to (26) as follows,

$$\begin{aligned}\phi^x=&\Bigg(8\Bigg[x^3A^2\overline{Q}^2(-d+\theta-z+3)r_F^{\frac{2\theta(d-2)}{d-1}}\pi^2(-2x^{z-1}x^{3-2d-2z+2\theta}(2-d-z+\theta)R^{\frac{z-\theta}{-1+\theta}}\\&+x^{z-2}x^{4-2d-2z+2\theta}R^{\frac{z-\theta}{-1+\theta}}(-d+\theta-z+1))\tau r_0^{\frac{\gamma(d-1)\lambda_3+(-2z+2)d+2z+2\theta-2}{d-1}}\\&+\Bigg[(-d+\theta+1)\omega_{k,d-1}^2Z_0(2x^{z-1}\tau(d-2)^2R^{\frac{z-\theta}{-1+\theta}}+x(R^{\frac{z-\theta}{-1+\theta}}\tau(-d+\theta-z+1)((-d+\theta-z+3)^2x^2+(d-2)^2)x^{z-2}\\&+4\pi(-d+\theta-z+3)^2))C^2\Bigg]\Bigg/\Big(128\Big)\Bigg]x^{d-\theta}\Bigg)\Bigg/\Big(C\omega_{k,d-1}A\pi(-d+\theta-z+3)^2Z_0x^3\tau\Big)\end{aligned} \tag{34}$$

$$\phi^{\Theta}=-\cot\Theta\csc\Theta \tag{35}$$

Also, we can calculate the τ as follows,

$$\begin{aligned}\overline{\tau}=&-\Big[4R^{\frac{-z+\theta}{-1+\theta}}(d-\theta-1)(d-\theta+z-3)\omega_{k,d-1}^2Z_0x^2\pi C^2\Big]\times\Big[128A^2x^{6-2d-z+2\theta}\overline{Q}^2r_F^{\frac{2\theta(d-2)}{d-1}}\pi^2(d-\theta+z-3)\\&\times r_0^{\frac{\gamma(d-1)\lambda_3+(-2z+2)d+2z+2\theta-2}{d-1}}-((d-\theta+z-1)(d-\theta+z-3)x^{2+z}+x^z(d-2)^2)C^2(d-\theta-1)Z_0\omega_{k,d-1}^2\Big]^{-1}\end{aligned} \tag{36}$$

In the classical or traditional framework, the standard approach to studying phase behavior involves identifying the critical point (critical boundary), which, depending on the structure of the equations derived from the model, typically either critical temperature or critical pressure is used. Once this boundary is established, phase behavior is examined on both sides by analyzing one of the free energy forms (Helmholtz or Gibbs) to determine whether the relevant function remains continuous or exhibits discontinuities.
Generally, due to the intrinsic relationship between temperature, pressure, and free energy, below the critical temperature, we observe sharp points and discontinuities, often forming a swallowtail structure, which indicates a first-order phase transition. Conversely, above this boundary, the system exhibits a smooth and continuous curve, signifying a second-order phase transition, where changes occur seamlessly without forming an unstable minimum energy state. Correspondingly, in the topological analysis of black hole phase behavior, different black hole configurations (small, intermediate, and large) manifest as zero points characterized by their topological charge. In a first-order phase transition, the unstable intermediate black hole typically exhibits a topological charge of -1, while the stable small and large black holes display charges of $+1$. Conversely, in a second-order phase transition, only one black hole state emerges, generally carrying a topological charge of $+1$. This distinct behavioral difference is also clearly reflected in the τ diagram.
In this study, instead of considering pressure or temperature as the critical parameter, we analyze the critical boundary in terms of central charge (C) or charge (Q) within the framework of CFT. By doing so, we aim to explore how phase behavior varies with these parameters, essentially play a more influential role in the CFT structure.
Considering the critical values obtained in Figs. 1-4 and considering the chosen values for Θ, we will carry out the topological study in three parts.

A. $\theta = 0.5$, $C_{crt} = 2.23$

Here, Given the central charge, we will witness a first-order phase transition at $C > C_{crt}$, and we will witness a second-order phase transition at $C < C_{crt}$.

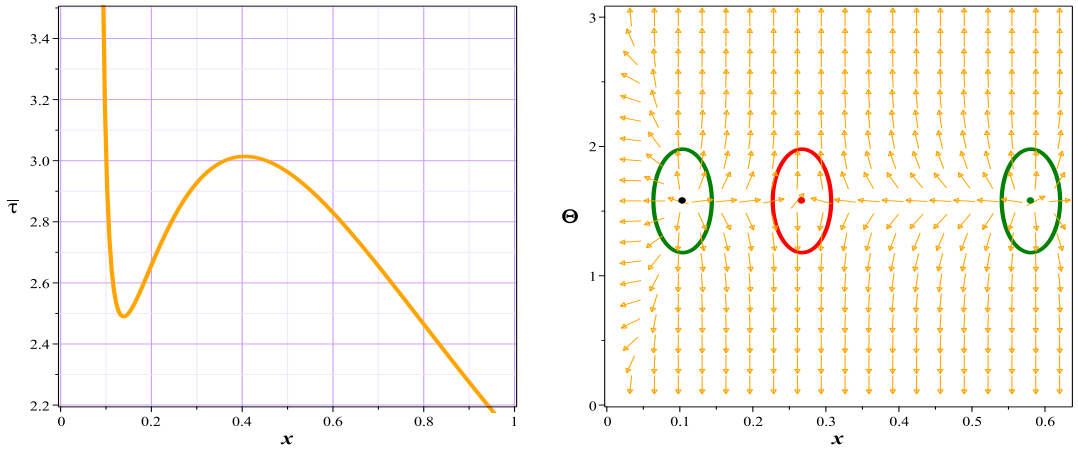

FIG. 7. The of curve $(x - \tau)$ (left plot) and the zero points (ZPs) are positioned at coordinates $(x - \Theta)$ (right plot) with $\overline{Q} = 0.001$, $k = Z_0 = \gamma = \lambda_3 = R = r_0 = r_F = A = \omega_{k,d-1} = 1$, $z = 3/2$, $d = 4$, $C = 7.9$, $\theta = 0.5$ with respect to $(\tau = 2.86)$ in $(x - \Theta) = (0.1038127759, \pi/2), (0.2672276612, \pi/2), (0.5807312771, \pi/2)$. **first-order phase transition**

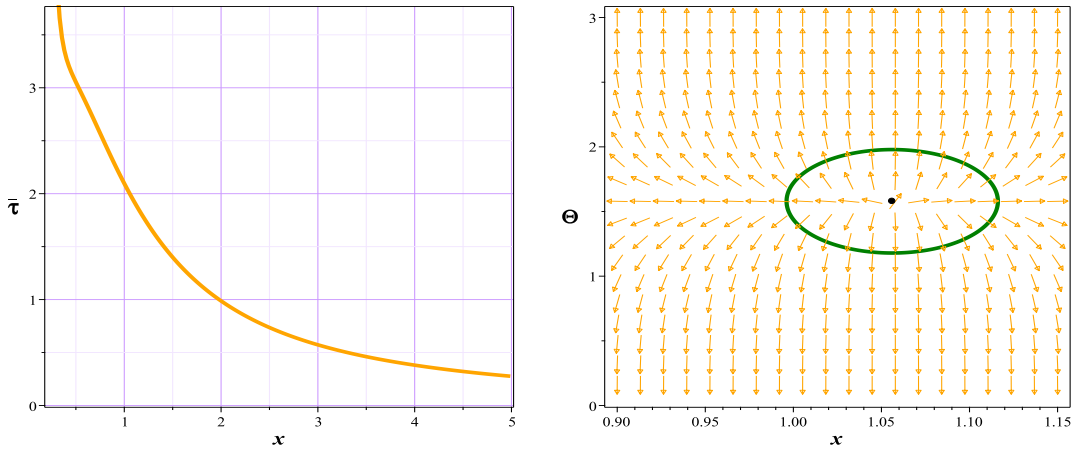

FIG. 8. The of curve $(x - \tau)$ (left plot) and the zero points (ZPs) are positioned at coordinates $(x - \Theta)$ (right plot) with $\overline{Q} = 0.001$, $k = Z_0 = \gamma = \lambda_3 = R = r_0 = r_F = A = \omega_{k,d-1} = 1$, $z = 3/2$, $d = 4$, $C = 0.9$, $\theta = 0.5$ with respect to $(\tau = 2)$ in $(x - \Theta) = (1.056127442, \pi/2)$. **second-order phase transition**

B. $\theta = 0$, $C_{crt} = 6.613$

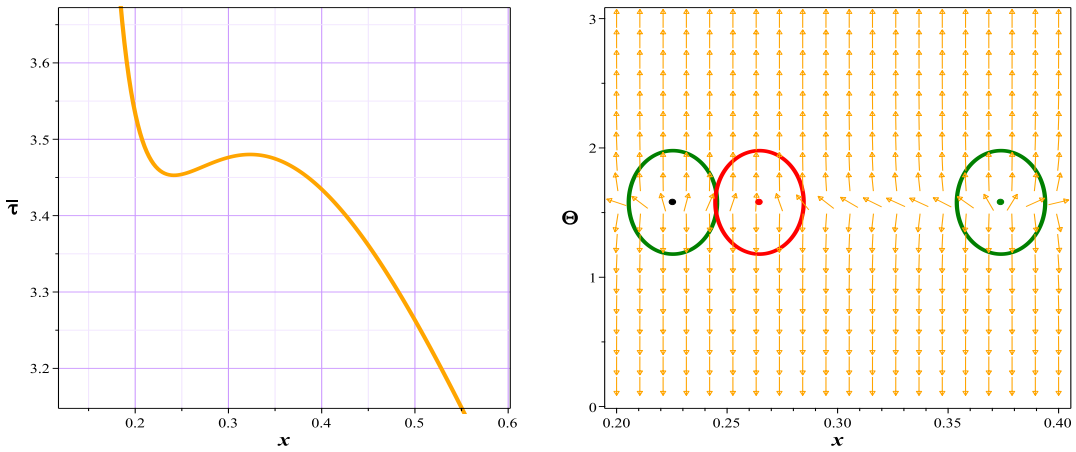

(a) (b)

FIG. 9. The of curve $(x-\tau)$ (left plot) and the zero points (ZPs) are positioned at coordinates $(x-\Theta)$ (right plot) with $\overline{Q} = 0.001$, $k = Z_0 = \gamma = \lambda_3 = R = r_0 = r_F = A = \omega_{k,d-1} = 1$, $z = 3/2$, $d = 4$, $C = 7.9$, $\theta = 0$ with respect to $(\tau = 3.46)$ in $(x-\Theta) = (0.2254889554, \pi/2), (0.2646634051, \pi/2), (0.3739296163, \pi/2)$. **first-order phase transition**

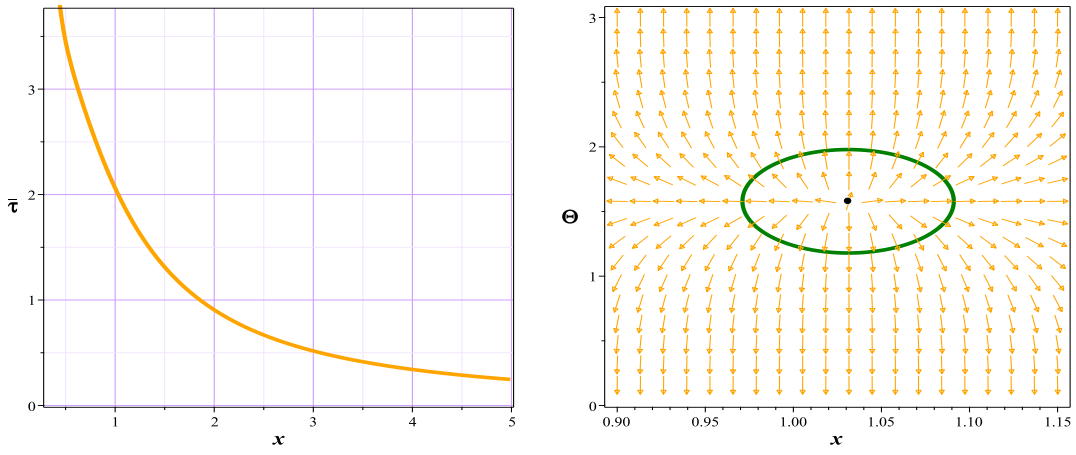

(a) (b)

FIG. 10. The of curve $(x-\tau)$ (left plot) and the zero points (ZPs) are positioned at coordinates $(x-\Theta)$ (right plot) with $\overline{Q} = 0.001$, $k = Z_0 = \gamma = \lambda_3 = R = r_0 = r_F = A = \omega_{k,d-1} = 1$, $z = 3/2$, $d = 4$, $C = 0.9$, $\theta = 0$ with respect to $(\tau = 2)$ in $(x-\Theta) = (1.031084358, \pi/2)$ **second-order phase transition**.

C. $\theta = -0.5$, $C_{crt} = 20.678$

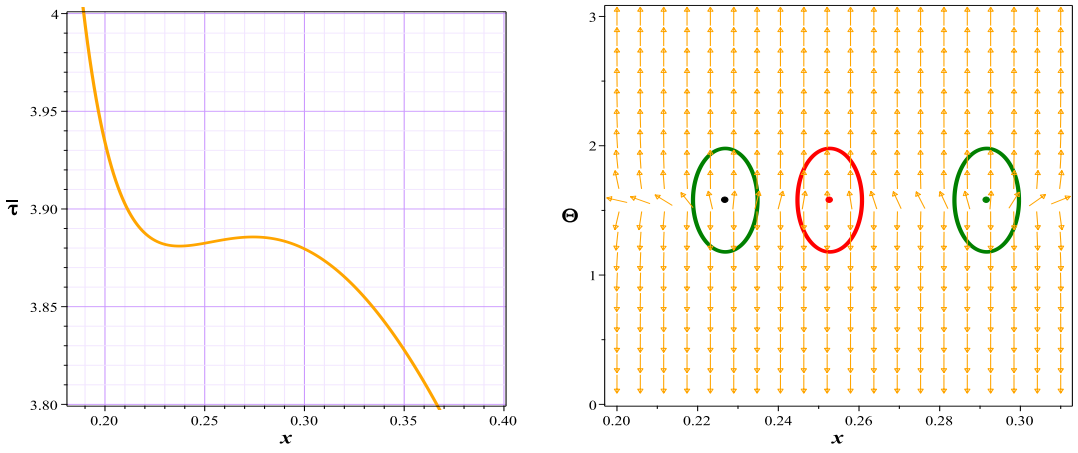

(a) (b)

FIG. 11. The of curve $(x-\tau)$ (left plot) and the zero points (ZPs) are positioned at coordinates $(x-\Theta)$ (right plot) with $\overline{Q} = 0.001$, $k = Z_0 = \gamma = \lambda_3 = R = r_0 = r_F = A = \omega_{k,d-1} = 1$, $z = 3/2$, $d = 4$, $C = 22$, $\theta = -0.5$ with respect to $(\tau = 2.3883)$ in $(x-\Theta) = (0.2268480364, \pi/2), (0.2527415340, \pi/2), (0.2916538929, \pi/2)$. **first-order phase transition**

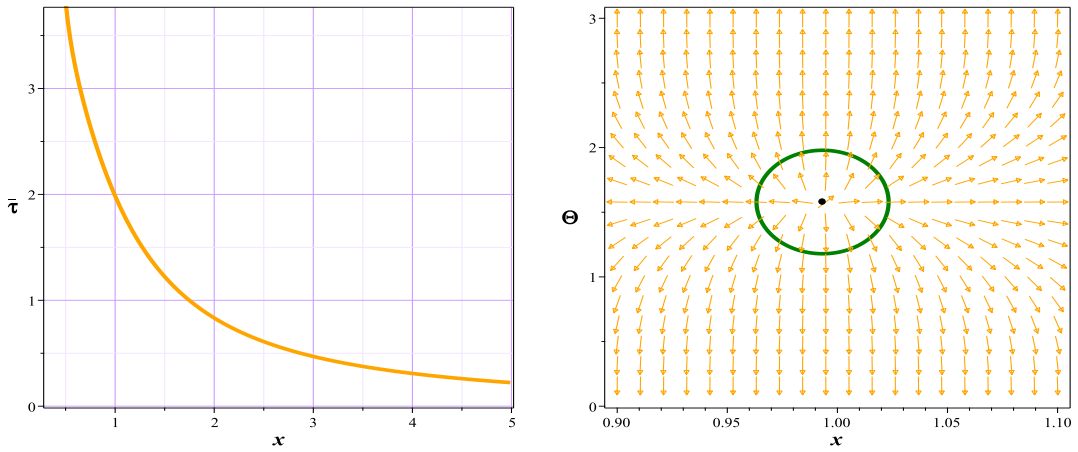

(a) (b)

FIG. 12. The of curve $(x-\tau)$ (left plot) and the zero points (ZPs) are positioned at coordinates $(x-\Theta)$ (right plot) with $\overline{Q} = 0.001$, $k = Z_0 = \gamma = \lambda_3 = R = r_0 = r_F = A = \omega_{k,d-1} = 1$, $z = 3/2$, $d = 4$, $C = 0.9$, $\theta = -0.5$ with respect to $(\tau = 2)$ in $(x-\Theta) = (0.9932587205, \pi/2)$. **second-order phase transition**

As shown in Figs. 7 to 12, for different values of the free parameter—particularly C—the topological charges and classification of black holes are determined. In general, the system exhibits a total topological charge of $W = +1$ in all cases, with the variation occurring in the number of topological charges. This difference is clearly reflected in the values of C. Specifically, when $C > C_{crt}$, the system possesses three topological charges ($\omega = +1, -1, +1$), with a total charge of $W = +1$, as seen in Figs. 7, 9, and 11 with first-order phase transition). Conversely, when $C < C_{crt}$, the number of topological charges is reduced, leaving only one topological charge ($\omega = +1$), as illustrated in Figs. 8, 10, and 12 with second-order phase transition), while the total charge remains $W = +1$.

V. CONCLUSION

To fully harness the power of the AdS/CFT correspondence, it is imperative to establish a well-defined set of translation rules that seamlessly connect gravitational-sector computations with their corresponding interpretations in the conformal field theory (CFT) framework. This systematic approach, commonly known as the holographic dictionary, serves as an intellectual conduit, enabling the bidirectional exchange of theoretical principles and computational insights. By formulating such dictionaries, researchers can extend fundamental ideas across these domains, fostering deeper exploration and broadening the scope of inquiry.

The development of a holographic dictionary specifically tailored for Lifshitz black holes and hyperscaling violation (HSV) models [1] has laid a crucial foundation for investigating CFT thermodynamics and the intricate phase structure of these black holes. Within this framework, our analysis will proceed through two distinct methodologies to provide a comprehensive understanding of their thermodynamic properties.

First, we employed the classical approach, identifying critical points and examining the behavior of the free energy function as a function of temperature near the critical boundary. This method enables us to characterize phase transitions and assess the stability of these models, shedding light on their equilibrium states and the underlying mechanisms governing their thermal behavior.

Next, to establish a comparative perspective and underscore the equivalence between these methodologies—particularly demonstrating the efficacy and accessibility of the topological approach—we extended our study to phase transitions through the formalism of topological charges. By leveraging this technique, we aim to refine our understanding of phase structures and thermodynamic properties in an intuitive and geometrically motivated manner.

Through this dual analysis, we provided a rigorous and insightful perspective on the thermodynamic attributes of Lifshitz black holes and HSV models, bridging classical and topological methodologies. Our findings will not only contribute to the broader discourse on black hole thermodynamics but also enhance the applicability of holographic techniques in exploring gravitational and quantum field theories.

Through a systematic examination of the thermodynamic properties of black holes within the framework of conformal field theory (CFT), we have characterized the intricate phase transitions influenced by electric charge ($\overline{Q}$) and central charge (C). Our analysis, based on figures 1–4, revealed that for $\overline{Q} < \overline{Q}_{crt}$, the free energy exhibits swallowtail behavior, indicating a first-order phase transition between two thermodynamically stable branches. As $\overline{Q} = \overline{Q}_{crt}$, the system undergoes a second-order phase transition, where a small stable black hole seamlessly transforms into a large stable black hole. Beyond this critical point ($\overline{Q} > \overline{Q}_{crt}$), no phase transition occurs. Similarly, examining variations in C, we determined that for $C > C_{crt}$, a first-order phase transition is observed, while at $C = C_{crt}$, the system undergoes a second-order transition. When $C < C_{crt}$, no transition takes place.

Additionally, our stability analysis, as presented in Figures 5 and 6, highlighted an intriguing contrast in the structural behavior of $\overline{Q}$ and C. While the system exhibits localized instability for $\overline{Q} < \overline{Q}_{crt}$ but remains stable otherwise, the opposite trend holds for C, where stability is maintained except for a narrow region at $C > C_{crt}$.

Moving beyond classical thermodynamic descriptions, we explored the topological structure of black hole phase transitions via the computation of topological charges (Figures 7–12). We established that while the total topological charge ($W = +1$) remains conserved across all scenarios, the number of individual topological charges varies depending on C. Specifically, when $C > C_{crt}$, the system possesses three distinct topological charges ($\omega = +1, -1, +1$), corresponding to a first-order phase transition. Conversely, when $C < C_{crt}$, the transition reduces to a second-order process with only a single topological charge ($\omega = +1$).

A complementary classification based on $\overline{Q}$ (Figures 13–18) reaffirms this structure: for $\overline{Q} < \overline{Q}_{crt}$, the system exhibits three topological charges, indicating a first-order phase transition, whereas for $\overline{Q} > \overline{Q}_{crt}$, only a single topological charge persists, marking a second-order transition.

These findings collectively demonstrate a robust correspondence between classical thermodynamic analysis and topological characterization of black hole phase transitions. The consistency in observed transitions validates the applicability of topological charge methods in identifying phase behavior, reinforcing the notion that black hole thermodynamics can be elegantly described through geometric and topological frameworks. This study not only advances our understanding of thermodynamic topology but also paves the way for future investigations into broader classes of gravitational systems exhibiting complex phase structures.

VI. APPENDIX

As previously stated, due to the distinct roles of the parameters $\overline{Q}$ and C in our analysis, we now provide explanations regarding the classification and number of topological charges associated with the black hole topology. As shown in Figs. 13 to 18, the topological charges and classification of black holes are determined based on different values of the free parameter—particularly $\overline{Q}$. In general, the system maintains a total topological charge of $W = +1$ in all cases, with the

variation occurring in the number of individual topological charges. This difference is directly influenced by the values of $\overline{Q}$. Specifically, when $\overline{Q} < \overline{Q}_{crt}$, the system exhibits three topological charges ($\omega = +1, -1, +1$), while the total charge remains $W = +1$. This behavior is illustrated in Figs. 13, 15, and 17, which correspond to first-order phase transitions. Conversely, when $C < C_{crt}$, the number of topological charges is reduced, leaving only a single topological charge ($\omega = +1$), as shown in Figs. 14, 16, and 18, which are associated with second-order phase transitions, while the total charge remains $W = +1$.

A. $\theta = 0.5, \overline{Q}_{crt} = 0.00269$

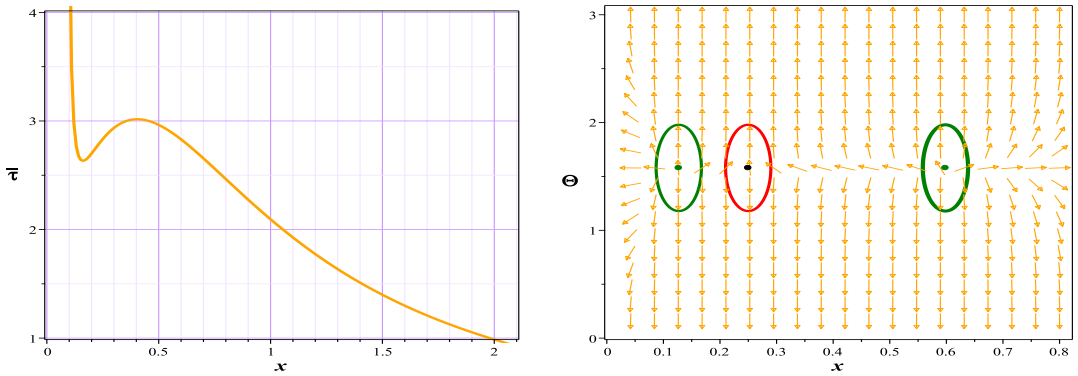

(a) (b)

FIG. 13. The of curve $(x - \tau)$ (left plot) and the zero points (ZPs) are positioned at coordinates $(x - \Theta)$ (right plot) with $C = 2$, $k = Z_0 = \gamma = \lambda_3 = R = r_0 = r_F = A = \omega_{k,d-1} = 1$, $z = 3/2$, $d = 4$, $\overline{Q} = 0.001$, $\theta = 0.5$ with respect to $(\tau = 2.833)$ in $(x - \Theta) = (0.1271852712, \pi/2), (0.2498976023, \pi/2), (0.5983782517, \pi/2)$. **first-order phase transition**

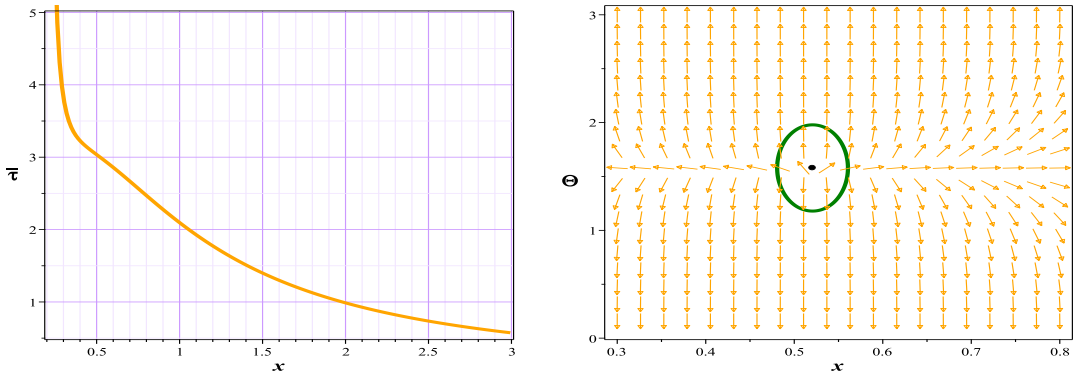

(a) (b)

FIG. 14. The of curve $(x - \tau)$ (left plot) and the zero points (ZPs) are positioned at coordinates $(x - \Theta)$ (right plot) with $C = 2$, $k = Z_0 = \gamma = \lambda_3 = R = r_0 = r_F = A = \omega_{k,d-1} = 1$, $z = 3/2$, $d = 4$, $\overline{Q} = 0.006$, $\theta = 0.5$ with respect to $(\tau = 3)$ in $(x - \Theta) = (0.5206801068, \pi/2)$. **second-order phase transition**

B. $\theta = 0, \overline{Q}_{crt} = 0.000907$

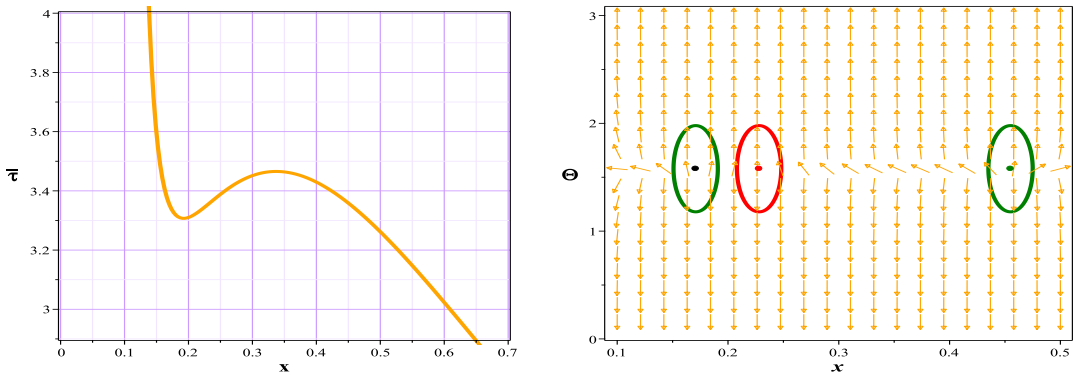

(a) (b)

FIG. 15. The of curve $(x - \tau)$ (left plot) and the zero points (ZPs) are positioned at coordinates $(x - \Theta)$ (right plot) with $C = 2$, $k = Z_0 = \gamma = \lambda_3 = R = r_0 = r_F = A = \omega_{k,d-1} = 1$, $z = 3/2$, $d = 4$, $\overline{Q} = 0.0005$, $\theta = 0$ with respect to $(\tau = 3.35)$ in $(x - \Theta) = (0.1708268874, \pi/2), (0.2280633172, \pi/2), (0.4550223997, \pi/2)$. **first-order phase transition**

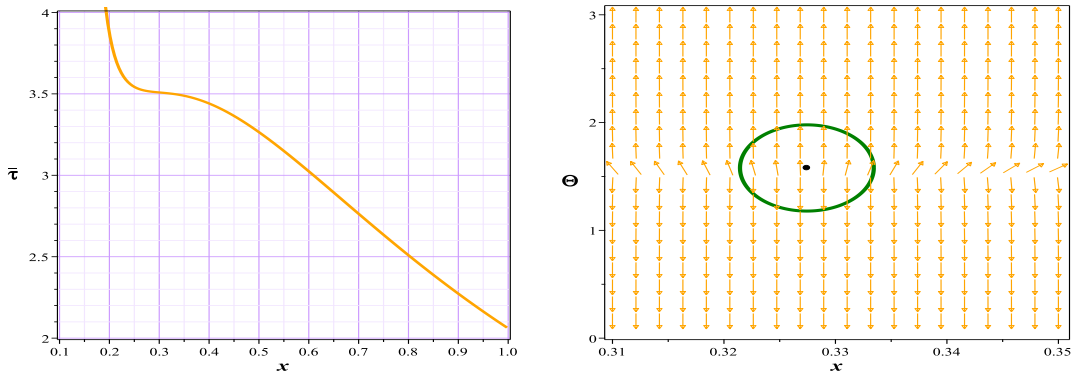

(a) (b)

FIG. 16. The of curve $(x - \tau)$ (left plot) and the zero points (ZPs) are positioned at coordinates $(x - \Theta)$ (right plot) with $C = 2$, $k = Z_0 = \gamma = \lambda_3 = R = r_0 = r_F = A = \omega_{k,d-1} = 1$, $z = 3/2$, $d = 4$, $\overline{Q} = 0.001$, $\theta = 0$ with respect to $(\tau = 3.5)$ in $(x - \Theta) = (0.3274380375, \pi/2)$. **second-order phase transition**

C. $\theta = -0.5, \overline{Q}_{crt} = 0.00029$

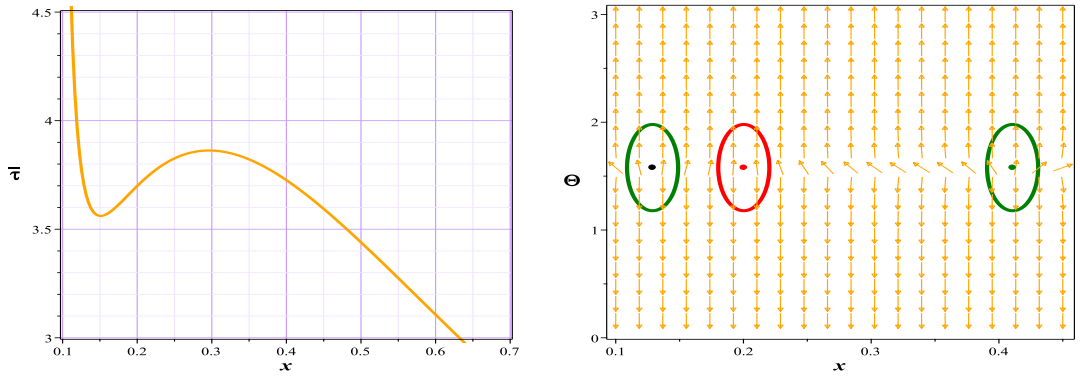

FIG. 17. The of curve $(x - \tau)$ (left plot) and the zero points (ZPs) are positioned at coordinates $(x - \Theta)$ (right plot) with $C = 2$, $k = Z_0 = \gamma = \lambda_3 = R = r_0 = r_F = A = \omega_{k,d-1} = 1$, $z = 3/2$, $d = 4$, $\overline{Q} = 0.0001$, $\theta = -0.5$ with respect to $(\tau = 3.7)$ in $(x - \Theta) = (0.1288450470, \pi/2), (0.2002584712, \pi/2), (0.4107284140, \pi/2)$. **first-order phase transition**

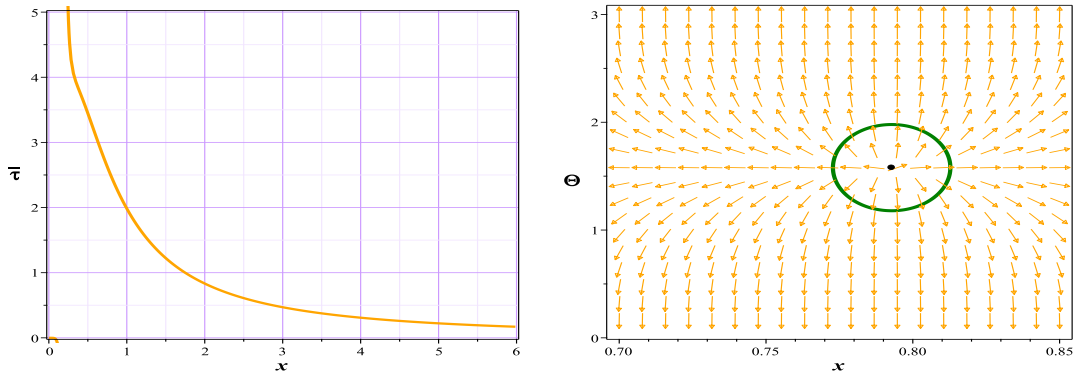

FIG. 18. The of curve $(x - \tau)$ (left plot) and the zero points (ZPs) are positioned at coordinates $(x - \Theta)$ (right plot) with $C = 2$, $k = Z_0 = \gamma = \lambda_3 = R = r_0 = r_F = A = \omega_{k,d-1} = 1$, $z = 3/2$, $d = 4$, $\overline{Q} = 0.001$, $\theta = -0.5$ with respect to $(\tau = 2.5)$ in $(x - \Theta) = (0.7927951285, \pi/2)$. **second-order phase transition**

[1] Cong, Wan, et al. "Holographic dictionary for Lifshitz and hyperscaling violating black holes." arXiv preprint arXiv:2410.16145 (2024).
[2] Witten E. Anti de Sitter space and holography. arXiv preprint hep-th/9802150. 1998 Feb 20.
[3] Kastor D, Ray S, Traschen J. Enthalpy and the mechanics of AdS black holes. Classical and Quantum Gravity. 2009 Sep 22;26(19):195011.
[4] Kastor D, Ray S, Traschen J. Chemical potential in the first law for holographic entanglement entropy. Journal of High Energy Physics. 2014 Nov;2014(11):1-7.
[5] Karch A, Robinson B. Holographic black hole chemistry. Journal of High Energy Physics. 2015 Dec;2015(12):1-5.
[6] Johnson CV. Holographic heat engines. Classical and Quantum Gravity. 2014 Oct 1;31(20):205002.
[7] Visser MR. Holographic thermodynamics requires a chemical potential for color. Physical Review D. 2022 May 15;105(10):106014.

[8] Cong W, Kubizňák D, Mann RB, Visser MR. Holographic CFT phase transitions and criticality for charged AdS black holes. Journal of High Energy Physics. 2022 Aug;2022(8):1-37.; Ahmed MB, Cong W, Kubizňák D, Mann RB, Visser MR. Holographic dual of extended black hole thermodynamics. Physical Review Letters. 2023 May 5;130(18):181401.

[9] Sadeghi J, Alipour MR, Afshar MA, Noori Gashti S. Exploring the phase transition in charged Gauss–Bonnet black holes: a holographic thermodynamics perspectives. General Relativity and Gravitation. 2024 Aug;56(8):93.

[10] Yang SJ, Ali MS, Wei SW, Liu YX. Holographic thermodynamics of a five-dimensional neutral Gauss–Bonnet AdS black hole. The European Physical Journal C. 2025 Apr;85(4):1-3.

[11] D. Kubiznak and R. B. Mann, P-V criticality of charged AdS black holes, J. High Energy Phys. 1207, 033 (2012), [arXiv:1205.0559[hep-th]].

[12] A. Chamblin, R. Emparan, C. V. Johnson, and R. C. Myers, Charged AdS Black Holes and Catastrophic Holography, Phys. Rev. D 60, 064018 (1999), [arXiv:hep-th/9902170].

[13] S. Gunasekaran, D. Kubiznak, and R. B. Mann, Extended phase space thermodynamics for charged and rotating black holes and Born-Infeld vacuum polarization, J. High Energy Phys. 1211, 110 (2012), [arXiv:1208.6251[hep-th]].

[14] Z. Gao and L. Zhao, Restricted phase space thermodynamics for AdS black holes via holography, Class. Quany.Grav. 39, 075019 (2022), [arXiv:2112.02386 [gr-qc]].

[15] Wei, Shao-Wen, Yu-Xiao Liu, and Robert B. Mann. "Black hole solutions as topological thermodynamic defects." Physical Review Letters 129.19 (2022): 191101.

[16] Wei, Shao-Wen, and Yu-Xiao Liu. "Topology of black hole thermodynamics." Physical Review D 105.10 (2022): 104003.

[17] Bai, Ning-Chen, Lei Li, and Jun Tao. "Topology of black hole thermodynamics in Lovelock gravity." Physical Review D 107.6 (2023): 064015.

[18] Yerra, Pavan Kumar, and Chandrasekhar Bhamidipati. "Topology of Born-Infeld AdS black holes in 4D novel Einstein-Gauss-Bonnet gravity." Physics Letters B 835 (2022): 137591.

[19] Sadeghi, Jafar, et al. "Bardeen black hole thermodynamics from topological perspective." Annals of Physics 455 (2023): 169391.

[20] Wu, D. "Topological classes of thermodynamics of the four-dimensional static accelerating black holes." Physical Review D 108.8 (2023): 084041.

[21] Wu, D, and Shuang-Qing Wu. "Topological classes of thermodynamics of rotating AdS black holes." Physical Review D 107.8 (2023): 084002.

[22] Sadeghi, Jafar, et al. "Bulk-boundary and RPS Thermodynamicsfrom Topology perspective." Chinese Physics C (2024).

[23] Wu, D, et al. "Topological classes of thermodynamics of the static multi-charge AdS black holes in gauged supergravities." arXiv preprint arXiv:2402.00106 (2024).

[24] Sekhmani, Yassine, et al. "Thermodynamic topology of Black Holes in $F(R)$-Euler-Heisenberg gravity's Rainbow." arXiv preprint arXiv:2409.04997 (2024).

[25] Gogoi, Naba Jyoti, and Prabwal Phukon. "Thermodynamic topology of 4D dyonic AdS black holes in different ensembles." Physical Review D 108.6 (2023): 066016.

[26] Hazarika, Bidyut, and Prabwal Phukon. "Thermodynamic topology of D= 4, 5 Horava Lifshitz black hole in two ensembles." Nuclear Physics B 1006 (2024): 116649.

[27] Sadeghi, Jafar, et al. "Topology of Hayward-AdS black hole thermodynamics." Physica Scripta 99.2 (2024): 025003.

[28] Sadeghi, Jafar, et al. "Thermodynamic topology and photon spheres in the hyperscaling violating black holes." Astroparticle Physics 156 (2024): 102920.

[29] Hazarika, Bidyut, and Prabwal Phukon. "Thermodynamic topology of black holes in f (R) gravity." Progress of Theoretical and Experimental Physics 2024.4 (2024): 043E01.

[30] Wu, D. "Topological classes of thermodynamics of the four-dimensional Lorentzian charged Taub-NUT spacetimes." The European Physical Journal C 83.7 (2023): 589.

[31] Hazarika, Bidyut, B. Eslam Panah, and Prabwal Phukon. "Thermodynamic topology of topological charged dilatonic black holes." arXiv preprint arXiv:2407.05325 (2024).

[32] Gashti, Saeed Noori, İzzet Sakallı, and Behnam Pourhassan. "Thermodynamic Topology, Photon Spheres, and Evidence for Weak Gravity Conjecture in Charged Black Holes with Perfect Fluid within Rastall Theory." arXiv preprint arXiv:2410.14492 (2024).

[33] Sadeghi, Jafar, and Mohammad Ali S. Afshar. "The role of topological photon spheres in constraining the parameters of black holes." Astroparticle Physics (2024): 102994.

[34] S. Afshar MA, Sadeghi J. Effective potential and topological photon spheres: a novel approach to black hole parameter classification. Chinese Physics C. 2024 May 29.

[35] Afshar, Mohammad Ali S., and Jafar Sadeghi. "Mutual Influence of Photon Sphere and Non-Commutative Parameter in Various Non-Commutative Black Holes: Part I-Towards evidence for WGC." arXiv preprint arXiv:2411.09557 (2024).

[36] Eslam Panah, B., B. Hazarika, and P. Phukon. "Thermodynamic topology of topological black hole in F (R)-ModMax gravity's rainbow." Progress of Theoretical and Experimental Physics 2024.8 (2024): 083E02.

[37] Wu, D. "Consistent thermodynamics and topological classes for the four-dimensional Lorentzian neutral NUT-charged spacetimes." The European Physical Journal C 83.5 (2023): 365.

[38] Wu, D. "Classifying topology of consistent thermodynamics of the four-dimensional neutral NUT-charged spacetimes." The European Physical Journal C 83.5 (2023): 365.

[39] Wu, Shan-Ping, and Shao-Wen Wei. "Thermodynamical topology of quantum BTZ black hole." Physical Review D 110.2 (2024): 024054.

[40] Sadeghi, Jafar, et al. "Bulk-boundary and RPS Thermodynamicsfrom Topology perspective." Chinese Physics C (2024).

[41] Sadeghi, Jafar, et al. "Thermodynamic Topology of Quantum Corrected AdS-Reissner-Nordstrom Black Holes in Kiselev Spacetime." Chinese Physics C (2024).
[42] Bidyut, Hazarika, and Prabwal Phukon. "Thermodynamic Properties and Shadows of Black Holes in f(R,T) Gravity." arXiv:2410.00606v1 (2024).
[43] Hemant Rathi, and Dibakar Roychowdhury. "Topology of black hole phase transition in JT gravity." arXiv:2410.00744 (2024).
[44] Gashti, Saeed Noori, et al. "Thermodynamic topology of Kiselev-AdS black holes within f (R, T) gravity." Chinese Physics C 49.3 (2025): 035110.
[45] Brzo, Aram Bahroz, et al. "Thermodynamic Topology of AdS Black Holes within Non-Commutative Geometry and Barrow Entropy." Nuclear Physics B (2025): 116840.
[46] Gashti, Saeed Noori, et al. "Thermodynamic topology and photon spheres of dirty black holes within non-extensive entropy." Physics of the Dark Universe (2025): 101833.
[47] Afshar, Mohammad Ali S., et al. "Topological Insights into Black Hole Thermodynamics: Non-Extensive Entropy in CFT framework.The European Physical Journal C 85 (4), (2025): 457.
[48] Gashti SN, Pourhassan B, Sakallı I. "Thermodynamic topology and phase space analysis of AdS black holes through non-extensive entropy perspectives." The European Physical Journal C. 2025 Mar 16;85(3):305.
[49] Gashti, Saeed Noori. "Topology of Holographic Thermodynamics within Non-extensive Entropy." Journal of Holography Applications in Physics 4 (4), 59-70 arXiv:2412.00889 (2024).
[50] Alipour, Mohammad Reza, et al. "Topological classification and black hole thermodynamics." Physics of the Dark Universe 42 (2023): 101361.
[51] Anand, Ankit, and Saeed Noori Gashti. "Universality relation and thermodynamic topology with three-parameter entropy model." Physics of the Dark Universe (2025): 101916.
[52] Gashti, Saeed Noori, and B. Pourhassan. "Non-extensive Entropy and Holographic Thermodynamics: Topological Insights. Eur. Phys. J. C 85, 435 (2025). " arXiv preprint arXiv:2412.12132 (2024).
[53] Afshar MA, Sadeghi J. WGC as WCCC protector: The synergistic effects of various parameters in non-commutative black holes for identifying WGC candidate models. Nuclear Physics B. 2025 May 1;1014:116872.
[54] Afshar MA, Sadeghi J. Mechanisms behind the Aschenbach effect in non-rotating black hole spacetime. Annals of Physics. 2025 Feb 11:169953.
[55] Heidari, N., I. P. Lobo, and V. B. Bezerra. "Gravitational signatures of a nonlinear electrodynamics in $f(R,T)$ gravity." arXiv preprint arXiv:2505.08718 (2025).
[56] Kachru S, Liu X, Mulligan M. Gravity duals of Lifshitz-like fixed points. Physical Review D—Particles, Fields, Gravitation, and Cosmology. 2008 Nov 15;78(10):106005.
[57] Danielsson UH, Thorlacius L. Black holes in asymptotically Lifshitz spacetime. Journal of High Energy Physics. 2009 Mar 10;2009(03):070.
[58] Dong X, Harrison S, Kachru S, Torroba G, Wang H. Aspects of holography for theories with hyperscaling violation. Journal of High Energy Physics. 2012 Jun;2012(6):1-33.
[59] Kastor, David, Sourya Ray, and Jennie Traschen. "Enthalpy and the mechanics of AdS black holes." Classical and Quantum Gravity 26.19 (2009): 195011.
[60] Tarrio, Javier, and Stefan Vandoren. "Black holes and black branes in Lifshitz spacetimes." Journal of High Energy Physics 2011.9 (2011): 1-27.
[61] Alishahiha, Mohsen, Eoin Ó. Colgáin, and Hossein Yavartanoo. "Charged black branes with hyperscaling violating factor." Journal of High Energy Physics 2012.11 (2012): 1-20.